Identification of atomic-like electronic states in indium arsenide nanocrystal quantum dots

Uri Banin*, **YunWei Cao***, **David Katz**† & **Oded Millo**†

* *Department of Physical Chemistry and the Farkas Center for Light Induced Processes,* † *Racah Institute of Physics, The Hebrew University, Jerusalem 91904, Israel*

....

Semiconductor quantum dots, due to their small size, mark the transition between molecular and solid-state regimes, and are often described as 'artificial atoms' (refs 1–3). This analogy originates from the early work on quantum confinement effects in semiconductor nanocrystals, where the electronic wavefunctions are predicted[4] to exhibit atomic-like symmetries, for example 's' and 'p'. Spectroscopic studies of quantum dots have demonstrated discrete energy level structures and narrow transition linewidths[5–9], but the symmetry of the discrete states could be inferred only indirectly. Here we use cryogenic scanning tunnelling spectroscopy to identify directly atomic-like electronic states with s and p character in a series of indium arsenide nanocrystals. These states are manifest in tunnelling current–voltage measurements as two- and six-fold single-electron-charging multiplets respectively, and they follow an atom-like Aufbau principle of sequential energy level occupation[10].

InAs nanocrystals for this study were prepared using a solution-phase pyrolytic reaction of organometallic precursors. These nanocrystals are nearly spherical in shape, with size controlled between 10 and 40 Å in radius[11]. The nanocrystal surface is passivated by organic ligands which also provide chemical accessibility for quantum dot (QD) manipulation: for example, to prepare "nanocrystal molecules"[12,13], nanocrystal-based light-emitting diodes[14], and to fabricate single-electron tunnelling devices[15]. For the tunnelling spectroscopy studies we link the nanocrystals to a gold film via hexane dithiol molecules[16].

Figure 1a (left inset) shows a scanning tunnelling microscope (STM) topographic image of an isolated InAs QD, 32 Å in radius. Also shown in Fig. 1a is a tunnelling current–voltage (I–V) curve that was acquired after positioning the STM tip above the QD and disabling the scanning and feedback controls, realizing a double-barrier tunnel junction (DBTJ) configuration[17–19] (Fig. 1a, right inset). A region of suppressed tunnelling current is observed around zero bias, followed by a series of steps at both negative and positive bias. In Fig. 1b we show the tunnelling conductance spectrum (that is, dI/dV versus V), which is proportional to the tunnelling density of states (DOS)[20]. A series of discrete single-electron tunnelling peaks is clearly observed, where the separations are determined by both single-electron charging energy (addition spectrum) and the discrete level spacings (excitation spectrum) of the QD. The I–V characteristics were acquired with the tip retracted from the QD to a distance where the bias voltage is dropped largely across the tip–QD junction. Under these conditions, conduction (valence) band states appear at positive (negative) sample bias, and the excitation peak separations are equal to the real QD level spacings[19].

On the positive-bias side of Fig. 1, two closely spaced peaks are observed immediately after current onset, followed by a larger spacing and a group of six nearly equidistant peaks. We attribute this doublet to tunnelling through the lowest conduction band QD state, where the spacing corresponds to the single-electron charging energy, $E_c = 0.11$ eV. The observed doublet is consistent with the degeneracy of the envelope function of the first conduction band
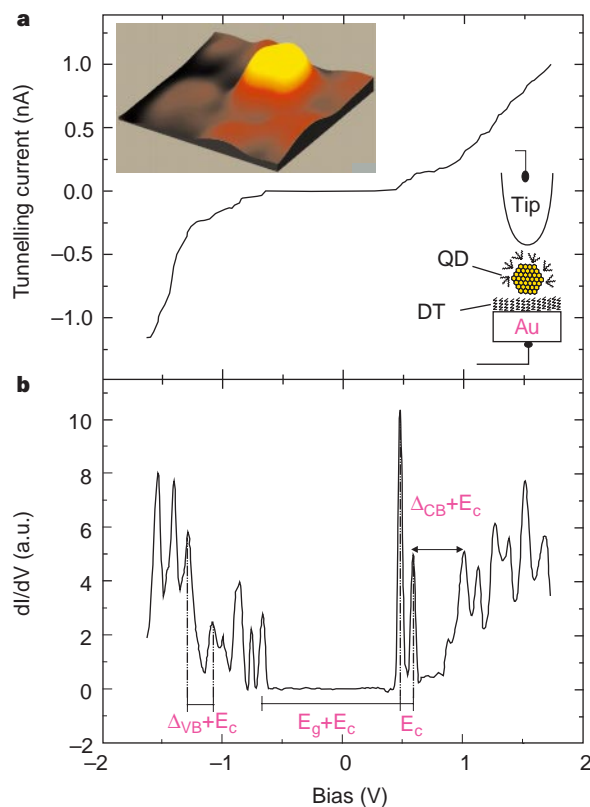

Figure 1 Scanning tunnelling microscopy and spectroscopy of a single InAs nanocrystal 32 Å in radius, acquired at 4.2 K. The nanocrystal quantum dots (QD) are linked to the gold substrate by hexane dithiol molecules (DT), as shown schematically in the right inset. Left inset, a 10×10 nm STM topographic image, showing the nanocrystal. For measuring the I–V characteristics, the STM tip was positioned above the QD, thus realizing a double-barrier tunnel junction configuration. **a**, The tunnelling I–V characteristic, exhibiting single-electron tunnelling effects. **b**, The tunnelling conductance spectrum, dI/dV versus V, obtained by numerical differentiation of the I–V curve (a.u., arbitrary units). The arrows depict the main energy separations: E_c is the single-electron charging energy, E_g is the nanocrystal bandgap, and Δ_{VB} and Δ_{CB} are the spacing between levels in the valence and conduction bands, respectively.

level, $1S_e$, which has s character. This direct relationship between multiplicity of a QD level and the number of addition peaks is substantiated by the observation that the second group consists of six peaks spaced by values close to the observed E_c for the first doublet. The degeneracy of the spherical atomic-like QD levels with envelope-function angular momentum l is $2(2l+1)$, including the electron spin. The second QD conduction band level, $1P_e$, has p character ($l = 1$) and can thus be occupied by six electrons. This sequential level filling resembles the Aufbau principle of building up the lowest-energy electron configuration of an atom[10], directly demonstrating the atomic-like nature of the QD.

The separation between the two groups of peaks, 0.42 eV, is a sum of the level spacing $\Delta_{CB} = 1P_e - 1S_e$, and the charging energy E_c. A value of $\Delta_{CB} = 0.31$ eV is thus obtained. On the negative-bias side, tunnelling through filled dot levels takes place, reflecting the tunnelling DOS of the QD valence band. Again, two groups of peaks are observed. The multiplicity in this case, in contrast with the conduction band, cannot be clearly assigned to specific angular momentum degeneracy. In a manner similar to that described above for the conduction band states, we extract a value of $\Delta_{VB} = 0.10$ eV for the level separation between the two observed valence band states.

In the region of null current around zero bias, the tip and substrate Fermi energies are located within the QD bandgap where the tunnelling DOS is zero. Tunnelling starts when the bias
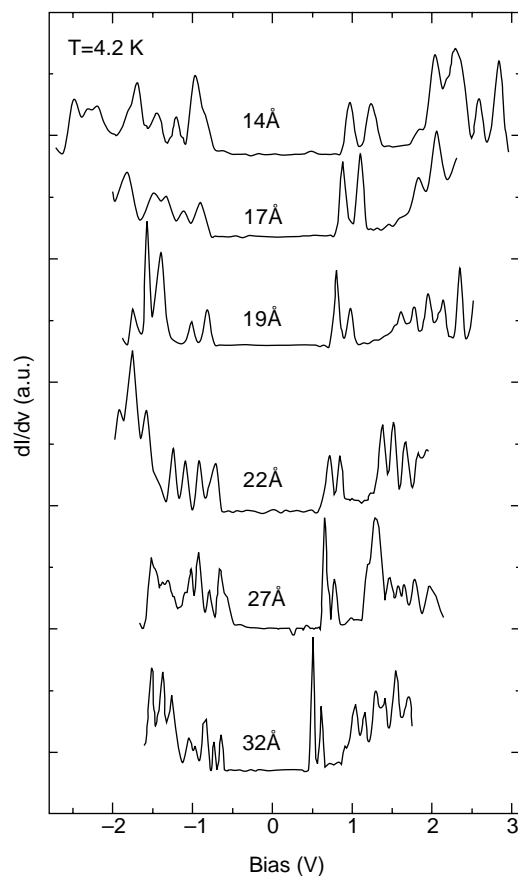
Figure 2 Size evolution of representative tunnelling dI/dV versus V characteristics, displaced vertically. The position of the centre of the observed zero-current gap showed non-systematic variations with respect to zero bias, of the order of 0.2 eV, probably due to variations of local offset potentials. For clarity of presentation, we offset the spectra along the V direction to situate the centres of the observed zero-current gaps at zero bias. The nanocrystal radii are denoted in the figure. The range of displayed voltage for each curve reflects the experimental saturation limit of the detected current.

is large enough to overcome both the bandgap, E_g, and charging energy. E_g is thus extracted by substracting E_c from the observed spacing between the highest valence band and lowest conduction band peaks, and is equal to 1.02 eV.

The tunnelling conductance spectra for single InAs nanocrystals of several radii are shown in Fig. 2. Two groups of peaks are persistently observed in the positive-bias side (conduction band). The first is always a doublet, consistent with the expected s symmetry of the $1S_e$ level, while the second has higher multiplicity of up to six, consistent with $1P_e$. (Partial indication of such behaviour was also observed previously on electrodeposited CdSe QDs[25].) The separation between the two groups, as well as the spacing of peaks within each multiplet, increase with decreasing QD radius. This reflects quantum size effects, on both the nanocrystal energy levels and its charging energy, respectively. On the negative-bias side, two groups of peaks, which exhibit similar quantum confinement effects are also observed. Here we find variations in the group multiplicities between QDs of different size, as well as variations of peak energy spacings within each group. This behaviour is partly due to the fact that the charging energy, E_c, is very close to the level spacing in the valence band Δ_{VB}, as shown in Fig. 3b. In this case, sequential single-electron tunnelling may be either addition to the same valence band state or excitation with no extra charging to the next state. An atomic analogy for this situation can be found in the changing order of electron occupation when
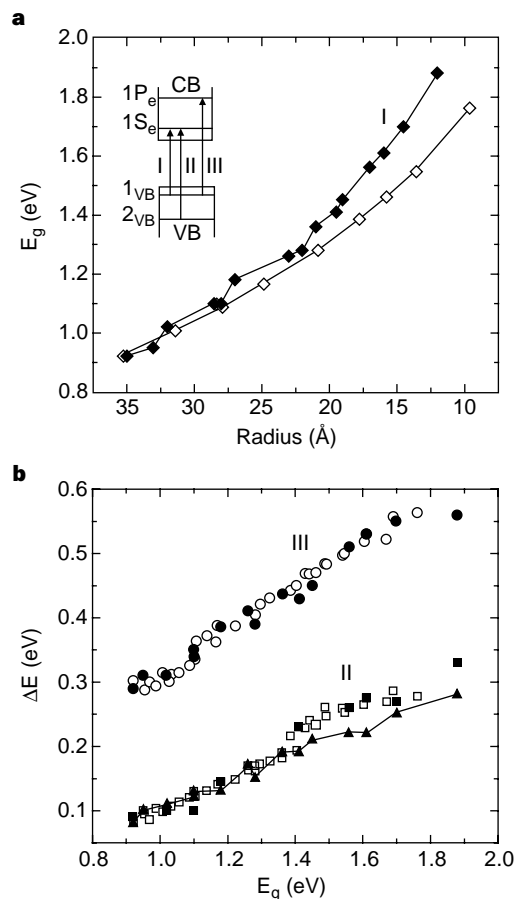

Figure 3 Correlation of optical and tunnelling spectroscopy data for InAs nanocrystals. Inset, diagram of the level structure of the conduction and valence bands, and the relevant strong optical transitions I, II and III. **a**, Comparison of the size dependence of the low-temperature optical bandgap (transition I) from which the excitonic Coulomb interaction was subtracted (open diamonds), with the bandgap measured by the STM (filled diamonds). **b**, Plot of excited transitions versus the bandgap for tunnelling and optical spectroscopy. The two lower data sets (II) depict the correlation between $\Delta_{VB} = 1_{VB} - 2_{VB}$, detected using the tunnelling spectroscopy as shown in Fig. 1b (filled squares), with the difference between transition II and the bandgap transition I (open squares). The two upper data sets (III) depict the correlation between $\Delta_{CB} = 1P_e - 1S_e$, determined using the tunnelling spectroscopy (filled circles), with the difference between optical transitions III and I (open circles). Also shown is the size dependence of the single-electron charging energy from the tunnelling data (filled triangles).

moving from the transition to the noble metals within a row of the periodic table. In the nanocrystals, as a consequence of the competition between charging and excitation, single-electron tunnelling through the first valence band state exhibits peak multiplicities that vary with size and do not necessarily correlate with the level multiplicity. Nevertheless, Δ_{VB} can be extracted from the wider peak spacing, which is due to both excitation and addition.

The tunnelling data can be further used to decipher the complex QD level structure through a correlation between spacings of levels observed in tunnelling-conductance spectra, with the allowed optical transitions as observed by photoluminescence excitation spectroscopy (PLE) of the InAs nanocrystals[9]. Complexities in the valence band levels of the nanocrystal result from the quantum-confinement-enhanced mixing of close-lying bulk semiconductor bands[21,22]. The mixing relaxes some of the optical transition selection rules, leading to rich and complex optical spectra of the nanocrystals[5,9,23]. The above correlation is also important when examining possible effects of charging and tip-induced electric field in the tunnelling measurements on the nanocrystal level structure.

We first compare the size dependence of the bandgap E_g, as extracted from the tunnelling data, with the nanocrystal sizing curve (Fig. 3a). The sizing curve (open diamond data points) was obtained by correlating the average nanocrystal size (that is, radius r), measured using transmission electron microscopy (TEM), with the excitonic bandgap of the same sample[9,24]. To compare these data with the tunnelling results, we have added a correction term, $1.8e^2/r$, to compensate for the electron–hole excitonic Coulomb interaction which is absent in the tunnelling data[4] (here e is the electron charge). Agreement is good for the larger nanocrystal radii, with increasing deviation for smaller nanocrystals. The deviation occurs because the TEM sizing curve provides a lower limit to the nanocrystal radius due to its insensitivity to the (possibly amorphous) surface layer. On the other hand, the size extracted from the STM topographic images is overestimated because of the tip–nanocrystal convolution effect[20]. These differences should be more pronounced for the small sizes, as is indeed observed.

Next, in Fig. 3b, we compare the size dependence of the higher strongly allowed optical transitions with the level spacings measured by tunnelling spectroscopy. We plot excited level spacings versus the observed bandgap for both PLE and tunnelling spectra, thus eliminating the problem of QD size estimation discussed above. The two lower data sets (II) in Fig. 3b compare the difference between the first strong excited optical transition and the bandgap from PLE (E3−E1 in ref. 9), with the separation $\Delta_{VB} = 2_{VB} - 1_{VB}$ in the tunnelling data (open and filled squares, respectively). The excellent correlation observed enables us to assign this first excited transition in the PLE to a $2_{VB} - 1S_e$ excitation, as shown schematically in the inset of Fig. 3. Strong optical transitions are allowed only between electron and hole states with the same envelope-function symmetry. We thus infer that the envelope function for state 2_{VB} should have s character and this state can be directly identified as the $2S_{3/2}$ valence band level[9].

Another important comparison is depicted by the higher pair of curves in Fig. 3b (set III). The second strong excited optical transition relative to the bandgap (E5−E1 in ref. 9) is plotted along with the spacing $\Delta_{CB} = 1P_e - S_e$ from the tunnelling spectra. Again, excellent correlation is observed, which allows us to assign this peak in the PLE to the $1_{VB}-1P_e$ transition (Fig. 3, inset). The top-most valence band level, 1_{VB}, should thus have some p character for this transition to be allowed. From this, and considering that the bandgap optical transition $1_{VB}-1S_e$ is also allowed, we conclude that 1_{VB} has mixed s and p character. It is not clear at present whether there is an intrinsic mixing[22] or degeneracy between different states having s and p characteristics[9]. Scanning tunnelling spectroscopy experiments in a magnetic field may resolve this issue.

The good correlation between optical transitions and the spacing of levels observed in the tunnelling spectra indicates that the charging did not have a significant effect on the QD level structure. The tunnelling I–V curves are thus well described as an algebraic sum of single electron charging energies and the QD level spacings. □

1. Alivisatos, A. P. Semiconductor clusters, nanocrystals, and quantum dots. *Science* **271**, 933–937 (1996).
2. Kastner, M. A. Artificial atoms. *Phys. Today* **46**, 24–31 (1993).
3. Ashoori, R. C. Electrons in artificial atoms. *Nature* **379**, 413–419 (1996).
4. Brus, L. E. Electron-electron and electron-hole interaction in small semiconductor crystallites. The size dependence of the lowest excited electronic state. *J. Chem. Phys.* **80**, 4403–4409 (1984).
5. Norris, D. J., Sacra, A., Murray, C. B. & Bawendi, M. G. Measurement of the size dependent hole spectrum in CdSe quantum dots. *Phys. Rev. Lett.* **72**, 2612–2615 (1994).
6. Leon, M., Petroff, P. M., Leonard, D. & Fafard, S. Spatially resolved visible luminescence of self-assembled semiconductor quantum dots. *Science* **267**, 1966–1968 (1995).
7. Gammon, D., Snow, E. S., Shanabrook, B. V., Katzer, D. S. & Park, D. Homogenous linewidths in the optical spectrum of a single gallium arsenide quantum dot. *Science* **273**, 87–90 (1996).
8. Empedocles, S. A., Norris, D. J. & Bawendi, M. G. Photoluminescence spectroscopy of single CdSe nanocrystallite quantum dots. *Phys. Rev. Lett.* **77**, 3873–3876 (1996).
9. Banin, U. *et al.* Size dependent electronic level structure of InAs nanocrystal quantum dots: Test of multiband effective mass theory. *J. Chem. Phys.* **109**, 2306–2309 (1998).
10. Herzberg, G. *Atomic Spectra and Atomic Structure* Ch. 3 (Prentice-Hall, New York, 1937).
11. Guzelian, A. A., Banin, U., Kadavanich, A. V., Peng, X. & Alivisatos, A. P. Colloidal chemical synthesis and characterization of InAs nanocrystal quantum dots. *Appl. Phys. Lett.* **69**, 1432–1434 (1996).
12. Mucic, R. C., Storhoff, J. J., Lestinger, R. L. & Mirkin, C. A. A DNA-based method for rationally assembling nanoparticles into macroscopic materials. *Nature* **382**, 607–609 (1996).
13. Alivisatos, A. P. *et al.* Organization of nanocrystal molecules using DNA. *Nature* **382**, 609–611 (1996).
14. Colvin, V. L., Schlamp, M. C. & Alivisatos, A. P. Light-emitting diodes made from cadmium selenide nanocrystals and a semiconductor polymer. *Nature* **370**, 354–357 (1994).
15. Klein, D. L., Roth, R., Lim, A. K. L., Alivisatos, A. P. & McEuen, P. L. A single electron transistor made from a cadmium selenide nanocrystal. *Nature* **389**, 699–701 (1997).
16. Colvin, V. L., Goldstein, A. N. & Alivisatos, A. P. Semiconductor nanocrystals covalently bound to metal surface with self-assembled monolayers. *J. Am. Chem. Soc.* **114**, 5221–5230 (1992).
17. Grabert, H. & Devoret, M. H. (eds) *Single Charge Tunneling* (Plenum, New York, 1992).
18. Alperson, B., Cohen, S., Rubinstein, I. & Hodes, G. Room-temperature conductance spectroscopy of CdSe quantum dots using a scanning force microscope. *Phys. Rev. B* **52**, R17017–R17020 (1995).
19. Porath, D., Levi, Y., Tarabia, M. & Millo, O. Tunneling spectroscopy of a single C₆₀ molecule in the presence of charging effects. *Phys. Rev. B* **56**, 9829–9833 (1997).
20. Wiesendanger, R. *Scanning Probe Microscopy and Spectroscopy* (Cambridge Univ. Press, 1994).
21. Ekimov, A. I. *et al.* Absorption and intensity-dependent photoluminescence measurements on CdSe quantum dots: assignment of the first electronic transitions. *J. Opt. Soc. Am. B* **10**, 100–107 (1993).
22. Fu, H. & Zunger, A. Excitons in InP quantum dots. *Phys. Rev. B* **57**, R15064–R15067 (1998).
23. Bertram, D., Micic, O. I. & Nozik, A. J. Excited state spectroscopy of InP quantum dots. *Phys. Rev. B* **57**, R4265–R4268 (1998).
24. Banin, U., Lee, J. C., Guzelian, A. A., Kadavanich, A. V. & Alivisatos, A. P. Exchange interaction in InAs nanocrystal quantum dots. *Superlattices Microstruct.* **22**, 559–567 (1997).
25. Alperson, B., Hodes, G., Rubinstein, I., Porath, D. & Millo, D. Energy level tunneling spectroscopy and single electron charging in individual CdSe quantum dots. *Appl. Phys. Lett.* (in the press).

Surface impact ionization of polar-molecule clusters through pickup of alkali atoms

C. R. Gebhardt, H. Schröder & K.-L. Kompa

Max-Planck-Institut für Quantenoptik, Hans-Kopfermann-Strasse 1, 85748 Garching, Germany

The observation that clusters of neutral H_2O (refs 1–4) or SO_2 (ref. 5) molecules, on impact with essentially any solid surface, can decay efficiently into positively and negatively charged fragments has defied explanation, not least because the kinetic energy per molecule can be much smaller than the molecular ionization potentials. Here we present a microscopic model of the charging mechanism, based on a mass analysis of charged SO_2 cluster fragments, which appears to be applicable to polar-molecule clusters more generally. Our mass spectra reveal that all positively charged fragments carry an alkali ion (sodium, potassium or caesium), whereas the negative fragments are simply $(SO_2)_n^-$. The yields of both charged species are comparable, and can be enhanced significantly by pre-treating the sample surface with additional alkali atoms. The key to charge separation in the clusters therefore appears to be the pickup of a neutral (but readily ionized) adatom during impact, followed by delocalization of the adatom's valence electron within the cluster and the subsequent collision-induced fragmentation of the cluster into charged pieces. This process could be of practical use in, for example, charge-pair generation and surface analysis; it may also be relevant to atmospheric ionization processes.

We performed the experiments in a conventional two-chamber molecular-beam apparatus (background pressure, 10^{-7} mbar). Clusters are produced by condensation in a seeded free-jet expansion through a pulsed nozzle (diameter 0.5 mm, typical pulse width 400 μs, stagnation pressure up to 20 bar). The cluster size distribution is measured with the retarding field technique[6] employing 30-eV electron impact ionization. The target is mounted in the second chamber perpendicularly to the beam axis, 300 mm downstream from the nozzle. We estimate that a fraction of 2×10^{-4} of the uncondensed particles leaving the nozzle arrive at the surface where